International Journal of Heat and Mass Transfer 115 (2017) 282–293

Contents lists available at ScienceDirect

International Journal of Heat and Mass Transfer

journal homepage: www.elsevier.com/locate/ijhmt

Heat transfer and particle migration in nanofluid flow around a circular bluff body using a two-way coupled Eulerian-Lagrangian approach

R. Deepak Selvakumar, S. Dhinakaran *

The Centre for Fluid Dynamics, Department of Mechanical Engineering, Indian Institute of Technology Indore, Khandwa Road, Simrol, Indore 453 552, M.P, India

ARTICLE INFO

Article history:
Received 23 February 2017
Received in revised form 18 July 2017
Accepted 21 July 2017

Keywords:
Circular cylinder
Nanofluids
Heat transfer
Discrete Phase Modeling (DPM)
Two-way coupling
Particle distribution

ABSTRACT

Nanofluids are engineered suspensions of fine nanoparticles in basefluids. Being a two-component system, different numerical approaches are available to model the thermo-fluidic behavior of nanofluids. In this study, a two-way coupled Eulerian-Lagrangian approach based Discrete Phase Modeling (DPM) has been used to numerically study the flow and heat transfer of nanofluids around a circular bluff body. A 2-D, laminar, steady and forced convective flow of Al_2O_3-H_2O nanofluid around a hot circular cylinder at a constant temperature has been considered. Governing equations of motion and energy transfer for the continuous phase (basefluid) were solved using a finite volume approach and the nanoparticles (discrete phase) were individually tracked in a Lagrangian reference frame by solving the particle force balance equation. Results are presented at $10 \leqslant Re \leqslant 40$ and particle volume fraction (ϕ) varying from 0% to 5%. Heat transfer performance of nanofluids is presented in terms of local and average Nusselt numbers. As expected, Nusselt numbers increased with increase in particle volume fraction and Reynolds number. Results indicated that the heat transfer characteristics are notably influenced by Brownian motion and thermophoresis. Effects of reflect and trap boundary conditions for the particulate phase at the cylinder wall, on heat transfer characteristics of nanofluids are also discussed. Special attention has been paid to the distribution of nanoparticles in the flow domain. It is noted that, nanoparticle distribution is non-homogeneous in the proximity of cylinder and in the recirculation region. This observation is in complete contradiction with the basic assumption of conventional Single Phase Modeling (SPM) approach. Results of DPM analysis significantly vary from that of the SPM approach. Furthermore, it is observed that nanofluids with smaller nanoparticles are capable of producing higher heat transfer rates.

1. Introduction

Flow and heat transfer around bluff bodies is a classical scenario, which is very common in several industrial applications such as electronic cooling, nuclear reactors, heat exchangers and thin wire probes and sensors [1]. Due to its industrial relevance and interesting flow behavior, this scenario is a renowned topic of research and numerous works are reported in available literature. The current state of the art of fluid flow and heat transfer over a bluff body are described in many review articles and books [2–5]. Recent advancements in technology has led to miniaturization, high power output and thus, resulting in a high heat flux density in several industrial devices. Hence, increasing the heat transfer efficiency has become the top priority in many industries. But, the performances of current heat transfer systems are limited by the low thermal conductivity of traditional industrial coolants such as air, water, engine oil and ethylene glycol. Nanofluids which are engineered suspensions of fine nanoparticles in conventional cooling liquids posses enhanced thermal conductivity and good stability. Owing to their superior thermal transport characteristics, nanofluids are promising coolants for several high heat flux applications such as electronic components, automobiles, nuclear reactors, energy storage devices and solar absorbers [6]. Thus, many researchers are involved in experimental and numerical attempts to study the thermo-fluidic behavior of nanofluids in a variety of applications.

Numerical investigation of nanofluid flow and heat transfer around bluff bodies is a trending topic in recent times. Flow and heat transfer characteristics of nanofluids are different from the basefluids due to their altered thermo-physical properties. A numerical study on forced convective heat transfer around a solid circular cylinder using nanofluids was carried out by Valipour and Ghadi [7]. Hamilton-Crosser [8] and Brinkman [9] models were used to determine the effective thermal conductivity and viscosity of nanofluids, respectively. An enhancement in heat transfer was

* Corresponding author.
E-mail address: ssdhinakar@gmail.com (S. Dhinakaran).

http://dx.doi.org/10.1016/j.ijheatmasstransfer.2017.07.103
0017-9310/

Nomenclature

$\boldsymbol{V}$	velocity vector in x or y direction [m s^{-1}]
C_p	specific heat [J kg^{-1} K^{-1}]
D	diameter of the cylinder [m]
d_p	diameter of the nanoparticle [m]
F, f	force [N]
h	heat transfer coefficient [W m^{-2} K^{-1}]
k	thermal conductivity [W m^{-1} K^{-1}]
K_B	Boltzmann constant [J K^{-1}]
m	mass [kg]
n	normal direction to the cylinder surface [m]
np	number of particles in a cell volume
Nu	Nusselt number
p	pressure [Pa]
Re	flow Reynolds number [J/kg K]
T	temperature [K]
t	time [s]
u, v	velocity components in x and y directions [m s^{-1}]
x, y	rectangular coordinate components [m]
A	surface area [m^2]
Pr	Prandtl number

Greek symbols

δV	cell volume [m^3]
δ	distance between particles [nm]
λ	fluid mean free path [m]
μ	dynamic viscosity [kg m^{-1} s^{-1}]
ν	kinematic viscosity [m^2 s^{-1}]
ϕ	nanoparticle volume fraction
ρ	density [kg m^{-3}]

Subscripts/superscripts

∞	far stream value
B	Brownian
D	drag
f	basefluid (continuous phase)
M	mean/average value
p	nanoparticle (discrete phase)
S	local/surface value
th	thermophoretic
w	wall

observed in nanofluids when compared to the basefluids. Nanofluids exhibited stronger vorticity than the basefluids. Similar observations were reported by Valipour et al. [10] in a study of nanofluid flow around a square cylinder. Vegad et al. [11] performed a numerical study on forced convective nanofluid flow around a circular cylinder in which Maxwell Garnett [12] and Brinkman models [9] were employed to calculate the effective properties of nanofluids. Synonymous observations of increased heat transfer while using nanofluids were reported. A numerical study on mixed convective heat transfer around a circular cylinder by Abu-Nada et al. [13] showcased that the heat transfer enhancement is a function of thermal conductivity and volume fraction of nanoparticles. Bing and Mohammed [14] performed a numerical study on upward laminar mixed convective flow around a circular cylinder. It was reported that nanoparticles with smaller diameters led to higher heat transfer rates. A numerical study on laminar nanofluid flow around a circular cylinder by Farooji et al. [15] exhibited that there exists an optimum particle volume fraction that gives the maximum heat transfer for a given nanoparticle diameter. Effect of nanoparticle shape on heat transfer enhancement was showcased by a numerical analysis of transient natural convective boundary layer flow past a vertical cylinder using nanofluids by Chamkha et al. [16]. Results indicated that nanofluids with spherical nanoparticles produced higher heat transfer rates. Notable aspect of this work is that, Brownian motion and thermophoresis were considered while determining the effective thermal conductivity of nanofluids. A detailed study on wake dynamics and heat transfer of nanofluids in forced and mixed convective flow past a circular cylinder at high Prandtl numbers was carried out by Sarkar et al. [17]. Results indicated that a stabilizing effect in flow and enhanced heat transfer rates were observed at higher Richardson numbers. Similar results were obtained in a numerical study of mixed convective flow around a circular cylinder using nanofluids [18]. Mixed convective nanofluid flow around a square cylinder was numerically studied by Sarkar et al. [19] and the results indicated that, a strong relation exists between the nanoparticle volume fraction and mean Nusselt number. Addition of nanoparticles to the basefluid resulted in more number of low frequency higher energy modes in a mixed convective flow around a square cylinder [20]. During a mixed convective vertical flow and heat transfer around a square cylinder using nanofluids, addition of nanoparticles to the basefluid caused a decrease in total entropy generation [21].

It is to be noted that, all the reported works on nanofluid flow around bluff bodies are based on Single Phase Modeling (SPM) approach. SPM considers nanofluids as homogeneous liquids with effective properties calculated using theoretical correlations. It is also hypothesized that the nanoparticles and basefluid move with the same velocity and exist in thermal equilibrium. It is arbitrarily assumed that the nanoparticle distribution is homogeneous through out the flow domain. Even though this approach is simpler and computationally cheap, accuracy of the results depend greatly on the theoretical models used for prediction of effective properties of nanofluids. Also in reality, nanofluids are heterogeneous suspensions of randomly moving nanoparticles in a basefluid (continuous phase). Several factors such as gravity, friction between the fluid and solid particles, thermophoresis, Brownian motion, sedimentation and dispersion co-exist with the main flow of nanofluids. Furthermore, a difference in velocity between the discrete phase (nanoparticles) and the continuous phase (basefluid) exists due to the difference in their densities. All these phenomena indicate that, basefluid and nanoparticles will not have same velocity and there will be a velocity slip between them [22]. Thus, it is clear that, it is necessary to classify nanofluids as a two-component system which brings up different approaches of Multi Phase Modeling (MPM) to numerically model the thermo-fluidic behavior of nanofluids. Different types of MPM models used for simulating nanofluids are (i) VOF (Volume of Fluid), (ii) Mixture model, (iii) Eulerian-Eulerian and (iv) Discrete Phase Model (DPM). Among the available multiphase models, mixture model is more commonly used due to its simplicity and relatively lesser computational expenses. Mixture model has been used to numerically analyze the nanofluid flow and heat transfer in several flow scenarios like horizontal straight tubes, curved tubes, lid driven cavity, inclined enclosure, shallow cavity and circular annulus by several researchers and convincing results were obtained [23–35]. Even though mixture model has been widely used, due to its ability to capture the effects of slip velocity; accuracy of the results are still

dependent on the theoretical models used for calculation of the effective properties. It is well known that, lack of universal models for predicting thermo-physical properties of nanofluids is still an unsolved problem.

Discrete Phase Model (DPM), which is based on Eulerian-Lagrangian approach, simulates the continuous phase (basefluid) using Eulerian approach; while the particles are individually tracked using Lagrangian trajectory analysis method [36–38]. The main advantage of DPM is that, it is independent of theoretical models or experimental data for determining the thermo-physical properties of nanofluids. Nanoparticles can be tracked individually and forces between the fluid and particles due to superposition of several effects (Brownian motion, thermophoresis and Saffman lift force, etc.) can be accounted. Few works on numerical study of nanofluid flow and heat transfer using DPM have been reported in literature. Bianco et al. [36] performed a numerical study on forced convective nanofluid flow in a circular tube and showed that the results of DPM vary significantly from that of the SPM. A numerical study of heat transfer and dispersion of nanoparticles in a gas-solid flow though a micro-channel using DPM revealed that the Brownian motion of nanoparticles is an important factor that determines the dispersion of nanoparticles in the flow field [37]. In another numerical study of nanofluid flow in a micro-channel by Aminfar and Motallebzadeh [38], it was reported that homogeneity of nanoparticle distribution decreased with increase in Reynolds number. A comparison of experimental and numerical results of turbulent nanofluid flow in a helically coiled tube by Bahremand et al. [39] showed that the results of DPM matched closely with the experimental results. Rashidi et al. [40] numerically modeled the nanofluid flow and heat transfer around a triangular obstacle using DPM. It was observed that Brownian motion played a major role in increasing the heat transfer of nanofluids. Furthermore, numerical studies of He et al. [41] and Tahir and Mital [42] proved that the results of DPM match well with the experimental results. Recently, a numerical study by Bovand et al. [43] on nanofluid flow in a duct using DPM revealed that the trap and reflect boundary conditions for the nanoparticles over the wall surface will have notable effects on the heat transfer and nanoparticle distribution.

From the above literature review, it seems important to investigate the capability of DPM in modeling the thermo-fluidic behavior of nanofluids, as only few works are reported in this area. Also, only a very limited information is available in the literature, on the influence of particle concentration distribution on performance of nanofluids [40,42,43]. Hence, in this study, a 2-D, laminar, steady forced convective flow of Al_2O_3-H_2O nanofluid around a circular cylinder has been simulated numerically using DPM based on a two-way coupled Eulerian-Lagrangian approach. Particular attention has been paid to the spatial distribution of nanoparticles around the cylinder and effects of trap and reflect boundary conditions are also discussed. Furthermore, the roles of Brownian motion and thermophoresis on heat transfer performance of nanofluids are also studied.

2. Problem definition and mathematical modeling

2.1. Problem statement

A 2-D, laminar and steady flow of Al_2O_3-H_2O nanofluid around an infinitely long cylinder of circular cross-section has been considered. The cylinder is of diameter D and is maintained at a constant temperature (T_w) higher than the ambient temperature (T_∞). The nanofluid at ambient temperature (T_∞) flows with an uniform velocity (U_∞) around the hot circular cylinder, in positive x-direction. Diameter of the cylinder is $D = 1$ cm and the inlet, top and bottom boundaries are placed at a distance 40D and the outlet is placed at distance of 120D away from the cylinder as graphically shown in Fig. 1. Following assumptions are made in the simulations carried out in this study.

- The wall temperature of the cylinder (T_w = 310 K) is higher than the fluid flow temperature (T_∞ = 300 K) and the cylinder exchanges heat with the surrounding fluid.
- Two-way coupling between the basefluid and nanoparticles has been considered.
- Representative particle model [44] has been employed.
- Thermo-physical properties of the basefluid (H_2O) and nanoparticle (Al_2O_3) are taken as presented in Table 1.
- As the volume fractions considered in this study are relatively low (< 5%), particle-particle direct collisions are ignored.
- However, particle-wall collisions are considered in this study and the restitution coefficients for reflect boundary condition is taken to be 1.0 and for trap condition as zero.

2.2. Governing equations

An Eulerian model is employed for the basefluid and particle trajectory analysis for the discrete phase is performed using a Lagrangian approach. A two-way coupling approach, in which the discrete phase (Al_2O_3 – nanoparticles) are considered to be carried by the continuous phase (H_2O – basefluid), has been adopted. The nanoparticles exchange momentum with the continuous phase by exerting drag. Thus, the interactions between the continuous phase and discrete phase are fully considered in the present study. Prime feature of the particles of size in nanometers is the Brownian motion. The small scale fluctuations in the continuous phase caused by the Brownian motion of nanoparticles are also considered in the Lagrangian tracking. The random dispersion of nanoparticles in the basefluid due to Brownian motion, thermophoresis and particle weight is accounted in the Lagrangian particle equation of motion. The steady state governing equations for the Eulerian-Lagrangian discrete phase model are expressed as follows [36].

2.2.1. Governing equations of the continuous phase

Continuity equation

$$\nabla \cdot (\rho \boldsymbol{V}) = 0 \tag{1}$$

Momentum equation

$$\nabla \cdot (\rho \boldsymbol{V}\boldsymbol{V}) = -\nabla P + \mu \nabla^2 \boldsymbol{V} + S_v \tag{2}$$

Energy equation

$$\nabla \cdot (\rho \boldsymbol{V} C T) = \nabla \cdot (k \nabla T) + s_h \tag{3}$$

Here, $\mathbf{V}, T, p$ and t are velocity vector (m s^{-1}), temperature (K), pressure (Pa) and time (s), respectively. ρ, μ, k and C are density (kg m^{-3}), viscosity (kg m^{-1} s^{-1}), thermal conductivity (W m^{-1} K^{-1}) and specific heat capacity (J kg^{-1} K^{-1}) of the basefluid, respectively. The terms S_v (kg m^{-2} s^{-2}) and S_h (W m^{-3}) in Eqs. (2) and (3) are the source terms for momentum and energy exchanges with the particles. These source terms are calculated as [45]:

$$S_v = \sum_{np} \frac{m_p}{\delta V} \frac{d\boldsymbol{V}_p}{dt} \tag{4}$$

$$S_h = \sum_{np} \frac{m_p}{\delta V} C_p \frac{dT_p}{dt} \tag{5}$$

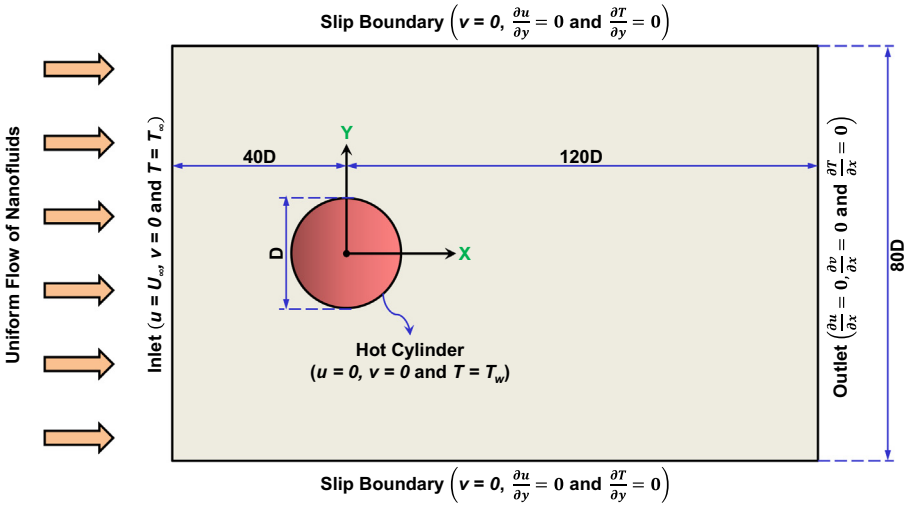

Fig. 1. Graphical view of the computation domain.

Table 1
Thermo-physical properties of the basefluid (water) and nanoparticles (Al_2O_3) [26].

S. no	Material	Thermal conductivity (W/m K)	Dynamic viscosity (kg/m s)	Density (kg/m^3)	Heat capacitance (J/kg K)
1	Al_2O_3	40	–	3970	765
2	H_2O	0.6	0.001003	997	4179

Here, δV is the cell volume, m_p is the mass of nanoparticles (kg) and np is the number of physical particles within a cell. The subscript p denotes the discrete phase (nanoparticles).

2.2.2. Governing equations of the discrete phase

Lagrangian particle trajectory analysis is employed to track the motion of individual particles. The particle inertia is balanced with other forces acting on the particles and accordingly, the equations of particle motion are given as [46]:

$$\frac{dX_p}{dt} = V_p \tag{6}$$

$$\frac{dV_p}{dt} = F_D(V_f - V_p) + \frac{g\left(\rho_p - \rho_f\right)}{\rho_p} + f_B + f_{th} \tag{7}$$

Here, subscripts p and f denote nanoparticle and basefluid, respectively and g is the acceleration due to gravity. The first term on the right hand side of the above equation indicates the drag force acting on the nanoparticles, second term represents the gravitational force acting on the particle due to its mass. The third and fourth terms indicate the Brownian force and thermophoretic force per unit mass, respectively.

The drag force is exerted on the particles by the continuous phase and hence, are carried by the continuous phase. This drag force on the nanoparticles is calculated by Stokes-Cunningham relation as

$$F_D = \frac{18\mu_f}{d_p^2 \rho_p C_c} \tag{8}$$

In Eq. (8), C_c is the Cunningham correction which is given as:

$$C_c = 1 + \frac{2\lambda}{d_p}\left[1.257 + 0.4e^{-(1.1d_p/2\lambda)}\right] \tag{9}$$

Here, λ indicates the mean free path (m). The thermophoretic force acting on the particles is given by the following relation.

$$f_{th} = -D_T \frac{1}{m_p T} \bigtriangledown T \tag{10}$$

In the above equation, T and m_p denote local fluid temperature (K) and particle mass (kg), respectively. D_T is the thermophoretic coefficient, which is calculated as [47]

$$D_T = 0.78 \frac{\pi \mu_f^2 d_p}{\rho_f} \frac{k_f}{2k_f + k_p} \tag{11}$$

The force acting on particles due to Brownian motion is determined as [46]

$$f_B = \zeta \sqrt{\frac{\pi S_0}{\Delta t}} \tag{12}$$

In the above equation, ζ is the zero mean unit-variance-independent Gaussian random number. The amplitudes of the Brownian force components are solved for each time step. Here, S_0 represents the spectral intensity of Brownian force (J kg^{-1} S^{-1}) and is calculated as:

$$S_0 = \frac{216 \nu K_B T}{\pi^2 \rho_f d_p^5 \left(\frac{\rho_p}{\rho_f}\right)^2 C_c} \tag{13}$$

Here, T is the absolute temperature of the fluid (K), ν is the kinematic viscosity (m^2 S^{-1}) and K_B is the Boltzmann constant (1.38×10^{-23} J K^{-1}). The energy equation for the particle is given as

$$m_p C_p \left(\frac{dT_p}{dt}\right) = hA(T_f - T_p) \tag{14}$$

In Eq. (14), C_p, A_p, T_f, T_p and h are heat capacity (J kg^{-1} K^{-1}) of the particle, surface area of the particle (m^2), local temperature of the basefluid, temperature of the particle and the convective heat trans-

fer coefficient (W m^{-2} K^{-1}). The convective heat transfer coefficient of the particle, h is given as [48]:

$$Nu_p = \frac{hd_p}{k_f} = 2 + 0.6Re_p^{0.5}Pr_f^{0.3} \tag{15}$$

In Eq. (15), Re_p is the particle Reynolds number based on the diameter of particle and the relative velocity. Pr_f and k_f are the Prandtl number and thermal conductivity (W m^{-1} K^{-1}) of the basefluid, respectively. It is to be noted that the particle-particle collisional heat transfer is not considered and only the fluid heat transfer affected by the source term is evaluated.

2.3. Boundary conditions

2.3.1. Boundary conditions for the basefluid (continuous phase)

Inlet

An uniform flow of basefluid is considered at the inlet of domain.

$$u = U_\infty, \quad v = 0, \quad \text{and} \quad T = T_\infty$$

Cylinder surface

No-slip boundary and constant wall temperature conditions are imposed on the cylinder surface.

$$u = 0, \quad v = 0, \quad \text{and} \quad T = T_w$$

Outlet

Outflow (zero gradient) boundary conditions are considered at the outlet of flow domain.

$$\frac{\partial u}{\partial x} = 0, \quad \frac{\partial v}{\partial x} = 0, \quad \text{and} \quad \frac{\partial T}{\partial x} = 0$$

Top and bottom boundaries

Symmetry conditions are applied on the top and bottom boundaries of computational domain.

$$v = 0, \quad \frac{\partial u}{\partial y} = 0, \quad and \quad \frac{\partial T}{\partial y} = 0$$

2.3.2. Boundary conditions for the nanoparticles (discrete phase)

At the inlet and outlet of the computational domain, escape type boundary condition has been applied. The particle trajectory tracking is terminated once the particles leave the computational domain. The inlet temperature of the particle is taken as 300 K. In this study, as we track the particles using a Lagrangian approach, it is necessary to consider the interaction of the particles with the cylinder wall. The particles may either stick to the cylinder surface or reflect from the cylinder surface. This interaction of particles with the cylinder surface is important, as they will influence the particle concentration in the proximity of cylinder. Typically, if a particle sticks to the cylinder surface, it is removed from the flow domain leading to a fall in concentration. This interaction of particles with the cylinder wall is studied by considering two types of boundary conditions for the particles at the cylinder surface, namely the reflect boundary condition with restitution coefficient as 1.0 or the trap boundary condition with a restitution coefficient of zero. In reflect boundary condition, the particle rebounds after hitting the cylinder wall with a momentum as defined by the restitution coefficient. Whereas, the particle sticks to the cylinder surface in a trap boundary condition. At the top and bottom boundaries of the computational domain, reflect boundary condition is applied.

2.4. Calculations of certain parameters

2.4.1. Local Nusselt number (Nu_S)

The local Nusselt on the circular cylinder surface is evaluated as

$$Nu_S = \frac{hD}{k_f} = -\frac{\partial T^*}{\partial n_S}\Big|_{on\ the\ cylinder\ surface} \tag{16}$$

Here, D represent the diameter of cylinder and n_s is the unit normal vector on the cylinder surface and "T^*" indicates non-dimensional temperature and is defined as:

$$T^* = \frac{T - T_\infty}{T_w - T_\infty} \tag{17}$$

2.4.2. Mean Nusselt number (Nu_M)

The local Nusselt number values have been further averaged over the entire cylinder surface to obtain the mean Nusselt number (Nu_M).

$$Nu_M = \frac{1}{\pi}\int_0^\pi Nu_S\, d\theta \tag{18}$$

2.4.3. Void fraction

The void fraction of each cell in the flow domain is evaluated as

$$\epsilon = 1 - \frac{\sum V_i}{\Delta V} \tag{19}$$

Here, V_i is the volume of ith particle in each cell of volume $\Delta V = \Delta x \Delta y d_p$. This indicates that the 2-D domain considered here is accounted as a pseudo 3-D domain with thickness equal to one particle diameter (d_p) [49].

3. Numerical methods and grid sensitivity analysis

The flow domain was modeled, meshed and necessary boundary conditions are set using the commercial preprocessor software ANSYS ICEM CFD 15.0. The commercial CFD software FLUENT 15.0 which is based on the control volume approach is used for solving the governing equations of flow and energy transfer. As stated earlier, governing equations of the continuous phase are coupled with the discrete phase by means of momentum and energy source terms. Pressure-velocity coupling is achieved by SIMPLE method. The convective terms are discretized using third-order accurate QUICK scheme, respectively. The Lagrangian particle equation is discretized by a modified Euler method. All equations are solved in sequential iterations and the solutions are considered to be converged when the residuals become less than 10^{-7}.

Detailed computations have been performed to choose a suitable grid which ensures the accuracy and stability of the numerical

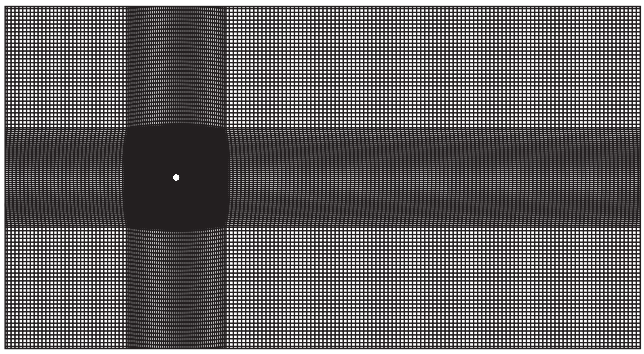

Fig. 2. Close view of the grid distribution near the cylinder.

solutions. A 2-D, non-uniform mesh has been used in the present study. Mesh distribution is more refined near the cylinder to capture the large variations and sharp gradients of flow and thermal field behavior near the cylinder, as seen in the close view of mesh shown in Fig. 2. Grid sensitivity analysis is carried out at $Re = 10, 40$ and $\phi = 2.5\%$, to ensure that the results presented in this study are independent of the effects of grid size. Three different grids with increasing fineness are tested. The results of grid sensitivity analysis are presented in Table 2. Based on the results of grid sensitivity analysis, 200×100 grid has been selected with the consideration of computational expenses and to ensure consistent numerical results.

4. Validation of the numerical results

The numerical code used in this study is validated by comparing with the results available in literature with air as working fluid ($Pr = 0.71$) at $10 \leqslant Re \leqslant 40$. Coefficient of drag and mean Nusselt number obtained from the present code is compared with the data of Lange et al. [2], Dennis and Chang [50] and Soares et al. [51]. From the comparison presented in Table 3, it is clear that the present results are in good agreement ($< 2\%$ variation) with the literature data and the results presented in this study are reliable.

5. Results and discussion

Flow and heat transfer of Alumina (Al_2O_3)-Water (H_2O) nanofluid flow around a circular cylinder is numerically analyzed using Discrete Phase Modeling (DPM) based on two-way coupled Eulerian-Lagrangian approach. The simulations are carried out in the following range of governing parameters.

Reynolds number (Re)	:	10, 20, 30 and 40.
Particle volume fraction (ϕ)	:	0–5%.
Particle diameter (d_p)	:	10, 20, 30, 40, 50 and 60 nm.

Simulation results for different values of parameters are presented in this section. Effects of different parameters on heat transfer performance in terms of isotherms, local and mean Nusselt numbers are presented. Variations in nanoparticle concentration distribution around the circular cylinder and particle trajectories are also discussed in detail. The heat transfer results obtained using the DPM approach are also compared with the results of SPM approach. The results of the SPM simulations presented in this study are based on the governing equations presented in an earlier study [52] and the effective properties of nanofluids are calculated by the theoretical models as described in [35].

5.1. Isotherms

The influences of particle volume fraction, nanoparticle diameter and boundary conditions for particles at the cylinder surface on the thermal field pattern around the circular cylinder is visualized by means of fluid phase isotherm contours in Figs. 3–5. Grid lines are provided to easily visualize the changes in lengths of isotherms and thickness of the thermal boundary layer. In general, it can be stated that the front surface of cylinder experiences higher transfer rates which is indicated by increased clustering of isotherms near the front stagnation point. In the rear side of the cylinder, thumb like projections of the thermal plume from the top and bottom surfaces of the cylinder are observed and the isotherms are relatively sparse. In the recirculation region, the center part of the thermal plume gets closer to the cylinder at rear stagnation point. Thermal field around the cylinder is symmetric about the top and bottom halves of the cylinder due to the symmetricity of the flow. Fig. 3 presents the isotherm contours at $\phi = 2.5\%$ and 5% at $Re = 40, d_p = 30$ nm and with reflect boundary conditions for the particles at the cylinder surface. It is seen that the thermal boundary layer is thin at $\phi = 5\%$ than at $\phi = 2.5\%$. This indicates the sharp temperature gradients and enhanced heat transfer at higher volume fractions. This increase in heat transfer at higher volume fractions can be a result of increase in effective thermal conductivity and increased particle–fluid interactions at higher volume fractions. Influence of nanoparticle diameter on distribution of isotherm contours around the circular cylinder at $Re = 40, \phi = 5\%, d_p = 10$ nm and 60 nm with reflect boundary condition for the nanoparticles at the cylinder surface is presented in Fig. 4. It is seen that the temperature gradients significantly decrease and the isotherms move away from the cylinder by increasing the particle diameter. This indicates a higher heat transfer rate at $d_p = 10$ nm when compared to $d_p = 60$ nm. It is apparently seen that the thermal boundary layer is very thin for nanofluids with smaller nanoparticles. The thumb like projections seen in the thermal plume are sharp and shorter at $d_p = 10$ nm. Whereas, a broad and longer thumb like projection of the thermal

Table 3
Comparison of present results with literature values of drag Coefficient (C_D) and mean Nusselt number (Nu_M) for $10 \leqslant Re \leqslant 40$ and $Pr = 0.71$.

Re	C_D	Nu_M	Authors
10	2.8047	1.8429	Present study
	2.8000	1.8100	Lange et al. [2]
	2.7600	1.8600	Soares et al. [51]
	2.8460		Dennis and Chang [50]
20	2.0256	2.4344	Present study
	2.0000	2.4100	Lange et al. [2]
	1.9900	2.4300	Soares et al. [51]
	2.0450		Dennis and Chang [50]
30	1.7020	2.8731	Present study
		2.8800	Lange et al. [2]
	1.6700	2.8500	Soares et al. [51]
40	1.5136	3.2372	Present study
	1.5000	3.2800	Lange et al. [2]
	1.4900	3.2000	Soares et al. [51]
	1.5220		Dennis and Chang [50]

Table 2
Grid sensitivity analysis using 2.5% nanofluid at $Re = 10$ and 40.

S. no	Re	Grid	C_D	% Difference	Nu_M	% Difference
1	10	200×100	2.8079	0.014	3.9571	0.06
2	10	400×200	2.8075	0.003	3.9596	0.02
3	10	600×300	2.8074	–	3.9607	–
4	40	200×100	1.5133	0.006	7.3864	0.03
5	40	400×200	1.5132	0.006	7.3888	0.03
6	40	600×300	1.5133	–	7.3912	–

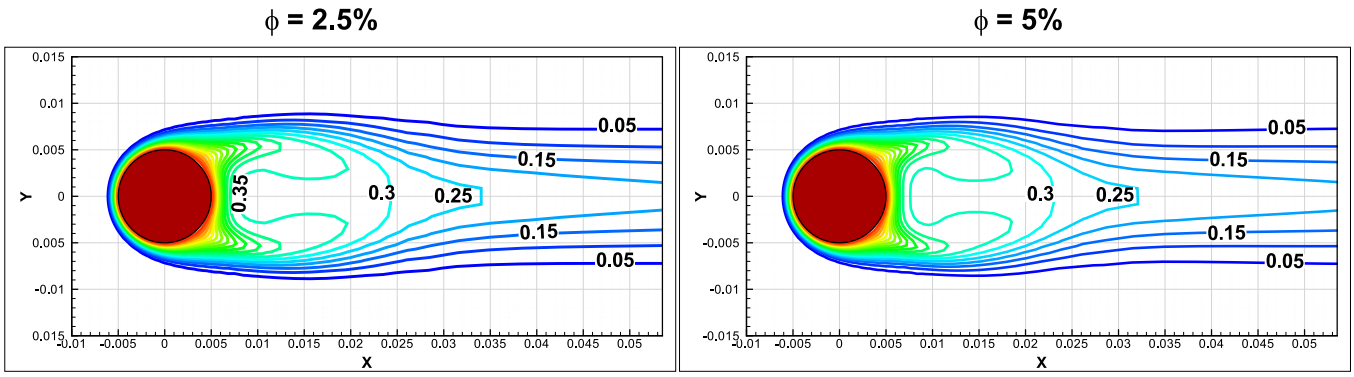

Fig. 3. Isotherm patterns for Al_2O_3-H_2O nanofluid flow around a circular cylinder at $\phi = 2.5\%$ and $5\%, d_p = 30$ nm and $Re = 40$ with reflect boundary condition for the particles at cylinder surface.

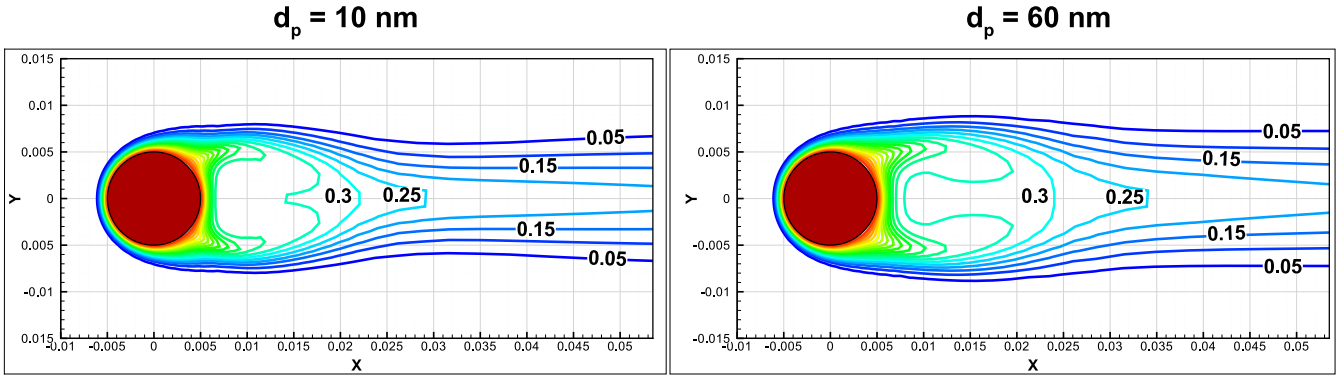

Fig. 4. Comparison of isotherm patterns for Al_2O_3-H_2O nanofluid flow around a circular cylinder with nanoparticle diameters $d_p = 10$ nm and 60 nm at $\phi = 5\%$ and $Re = 40$ with reflect boundary condition for the particles at cylinder surface.

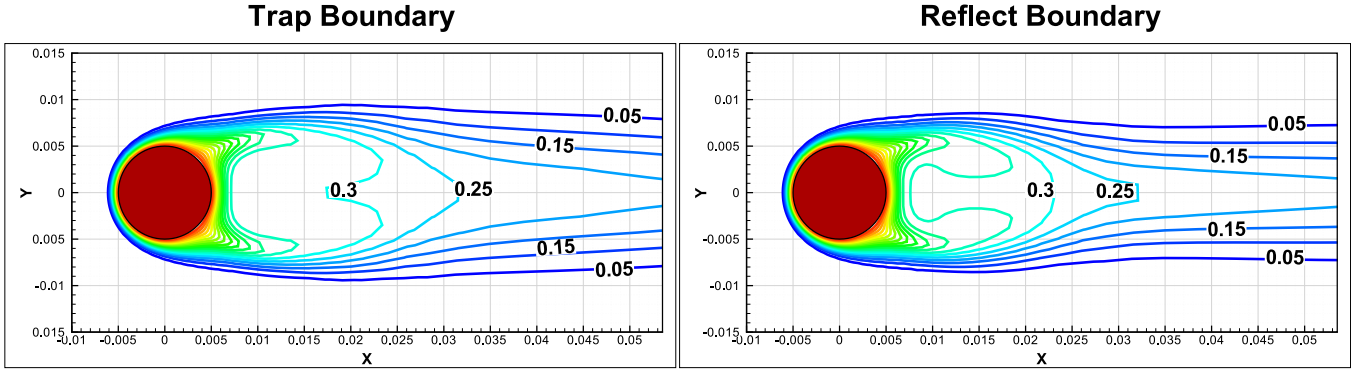

Fig. 5. Thermal field pattern around a circular cylinder for Al_2O_3-H_2O nanofluid flow around a circular cylinder at $\phi = 5\%, d_p = 30$ nm and $Re = 40$ with reflect and trap boundary conditions.

plume is seen at $d_p = 60$ nm. This increase in heat transfer at smaller nanoparticle diameters can be due to the higher surface to volume ratio of smaller nanoparticles and uniform distribution of smaller nanoparticles when compared to the larger nanoparticles [40]. It is to be noted that the type of boundary condition for the particles at the cylinder surface also influences the thermal field pattern around the cylinder. Fig. 5 shows the isotherm contours around the circular cylinder at $Re = 40, \phi = 5\%$ and $d_p = 30$ nm with reflect and trap boundary conditions for the particles at the cylinder surface. The isotherms are stretched in the linear direction and become closer to cylinder in the vertical direction with a clearly visible thinning of thermal boundary layer while using reflect boundary condition for the particles at cylinder surface. This indicates that the reflect boundary condition for the particles at the cylinder surface results in higher heat transfer rates than the trap boundary condition. This can be attributed to the increase in particle concentration around the cylinder surface when reflect boundary condition is applied. Whereas, a marginal fall in particle concentration is observed near the cylinder while trap boundary condition is used for the particles at the cylinder surface [40].

5.2. Local Nusselt number (Nu_S)

Distribution of local Nusselt numbers along the cylinder surface at $Re = 40, d_p = 30$ nm and at different particle volume fractions ($0\%, 2.5\%$ and 5%) with reflect boundary condition for the parti-

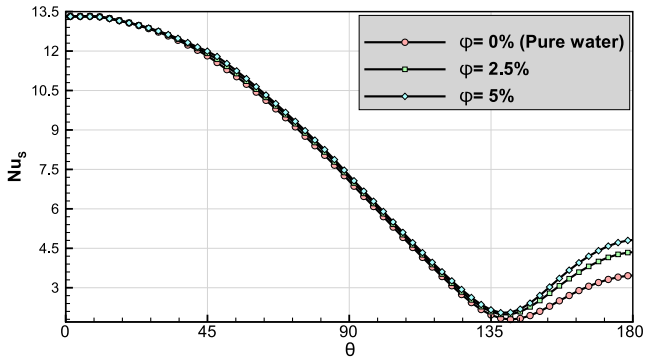

Fig. 6. Distribution of local Nusselt number (Nu_S) around the cylinder surface for Al_2O_3-H_2O (ϕ = 0%, 2.5% and 5%) nanofluid flow at $Re = 40, d_p = 30$ nm and with reflect boundary condition for the particles at cylinder surface.

cles at the cylinder surface are presented in Fig. 6. As the flow is symmetric about the top and bottom halves of the circular cylinder, the distribution of local Nusselt number is also symmetric. Thus, the local Nusselt number distribution is shown only for the top half of the circular cylinder ($\theta = 0^\circ$(front stagnation point) to 180° (rear stagnation point)). As seen in the figure, local Nusselt number values are highest at the front stagnation point and gradually fall towards the rear stagnation point. Thus, it can be inferred that the maximum heat transfer is experienced at the front stagnation point and it gradually decreases as the flow proceeds towards the rear end of the cylinder. At $\theta = 135^\circ$ (approx), a sudden increase in local Nusselt number values is noted up to $\theta = 180^\circ$. This increase in heat transfer near the rear stagnation point is due the recirculation wakes formed behind the cylinder. It is obvious that the local Nusselt numbers for nanofluids are higher than that of the pure basefluid. This can be attributed to the increase in effective thermal conductivity due to addition of nanoparticles and the Brownian motion of nanoparticles which results in enhanced heat transfer. It is necessary to mention that the effect of addition of nanoparticles on local Nusselt numbers is very minimum in the front and top surfaces of the cylinder. Whereas, in the recirculation region a notable increase in local Nusselt number is observed by increasing the particle volume fraction. This notable difference in local Nusselt number distribution in the recirculation region is due to the sharp variations in the nanoparticle distribution in this region at different volume fractions. This is synonymous to the observations of Afshar et al. [37], during a numerical study of nanofluid flow in a micro-channel, where the nanoparticle distribution significantly influenced the heat transfer rates.

5.3. Mean Nusselt number (Nu_M)

The heat transfer performance of nanofluids flowing around the circular cylinder is presented in terms of mean Nusselt number. The effects of Reynolds number, particle volume fraction, nanoparticle diameter, boundary condition for the particles at the cylinder surface, thermophoresis, Brownian motion and modeling approach are presented in Figs. 7–11. In Fig. 7, it is observed that the mean Nusselt number linearly increases by increasing the Reynolds number. The lowest value of mean Nusselt number for any particle volume fraction is seen at $Re = 10$ and the highest value is seen at $Re = 40$. The increased velocities at higher Reynolds numbers result in thinner boundary layer, that leads to easier and higher heat transfer rates. At any given Reynolds number, the heat transfer rates increased with increase in nanoparticle volume fraction. This indicates the effectiveness of nanofluid as a efficient cooling liquid. Addition of nanoparticles resulted in an increase in heat transfer which is indicated by the increase in mean Nusselt number. A 5.6% increase in mean Nusselt number is seen at $\phi = 5\%$ and $Re = 40$, when compared to the pure water. This increase in heat transfer observed at higher volume fraction of nanoparticles, can be attributed to several factors such as mixing effect brought out by the nanoparticles suspended in the basefluid, Brownian motion of nanoparticles inside the basefluid that leads to a pseudo-convection, thermal conductivity enhancement due to addition of nanoparticles, particle migration and thermophoresis, etc. The effect of nanoparticle diameter on mean Nusselt number at $Re = 40$ and $\phi = 5\%$ is shown in Fig. 8. Results indicate that smaller nanoparticles lead to higher mean Nusselt numbers indicating higher heat transfer rates. Nanofluids with 10 nm particles resulted in 7.7% higher heat transfer rate than the nanofluids with 60 nm particles. This is due to the fact that, smaller nanoparticles exhibit higher Brownian motion leading to augmented solid–liquid interactions, which result in enhanced heat transfer. Also, smaller nanoparticles result in more uniform distribution leading to better heat transfer rates [40]. Furthermore, smaller diameter means more number of nanoparticles at same volume fraction and hence, the interactions between the fluid and particles are more intense when compared to larger particles. As the heat transfer between particles and the basefluid takes places at the fluid interface, the thermal conductivity enhancement at a given volume fraction is higher for nanofluids with smaller nanoparticles. This is due to the higher surface to volume ratio of smaller nanoparticles [53]. The type of boundary condition for the particles at cylinder surface also influenced the mean Nusselt number. The effect of reflect and trap boundary conditions for the particles at cylinder surface at $10 \leqslant Re \leqslant 40$ and $\phi = 5\%$ is presented in Fig. 9. It is seen that the

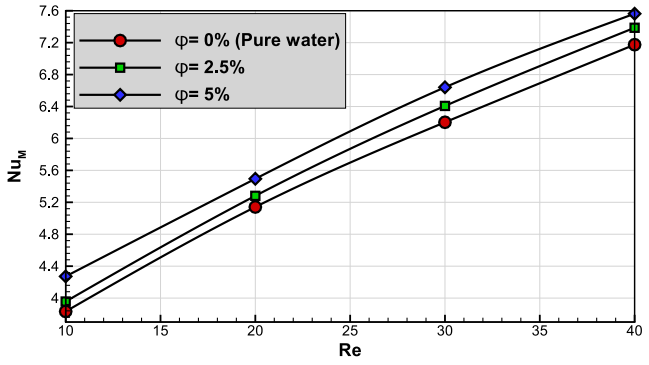

Fig. 7. Mean Nusselt number (Nu_M) variation for Al_2O_3-H_2O (ϕ = 0%, 2.5% and 5%) nanofluid flow around a circular cylinder at $10 \leqslant Re \leqslant 40$ and with reflect boundary condition for the particles at cylinder surface.

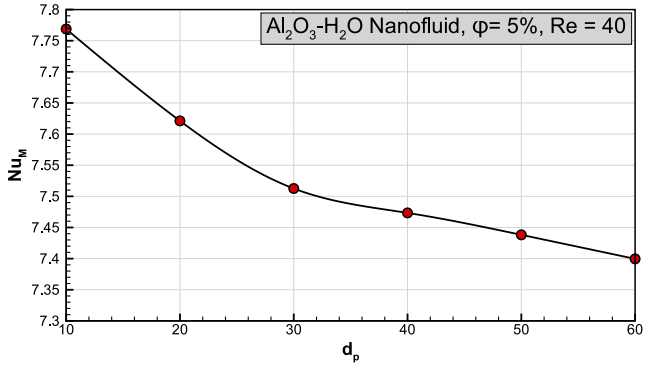

Fig. 8. Effect of particle diameter (d_p) on Mean Nusselt number (Nu_M) for Al_2O_3-H_2O (ϕ = 5%) nanofluid flow around a circular cylinder (reflect boundary) at $Re = 40$ with 10 nm $\leqslant d_p \leqslant$ 60 nm.

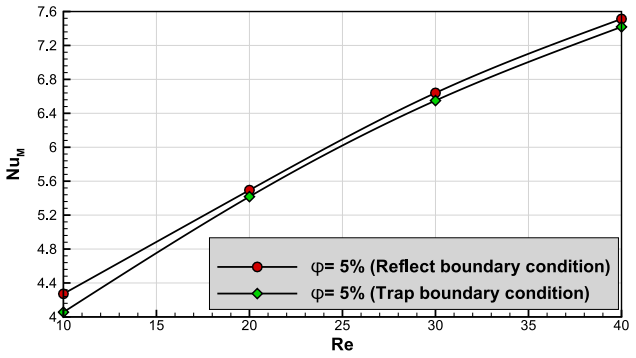

Fig. 9. Effect of reflect and trap boundary conditions for the particles at cylinder surface on mean Nusselt number (Nu_M) at $10 \leqslant Re \leqslant 40$ and $\phi = 5\%$ for Al_2O_3-H_2O nanofluid flow around a circular cylinder.

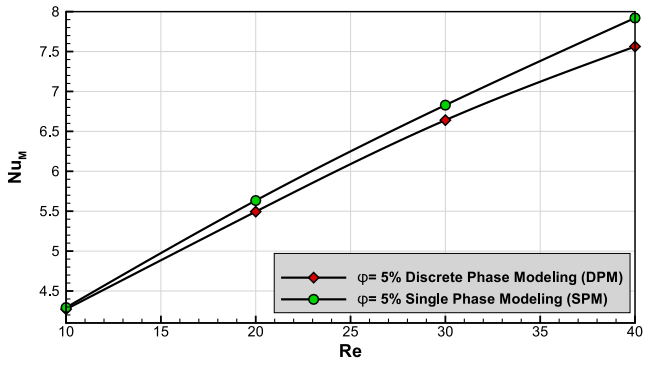

Fig. 11. Comparison of Mean Nusselt number (Nu_M) at $10 \leqslant Re \leqslant 40$ and $\phi = 5\%$ obtained using Discrete Phase Modeling (DPM) and Single Phase Modeling (SPM) of Al_2O_3-H_2O nanofluid flow around a circular cylinder.

reflect boundary condition resulted in higher mean Nusselt numbers than the trap boundary condition. Approximately, a 1.5% decrease in mean Nusselt number is seen while using trap boundary condition. This can be attributed to the marginal decrease in particle volume fraction while using trap boundary condition [43]. It is known that Brownian motion and thermophoresis are two important mechanisms that influence the thermal transport in nanofluids. The effect of these two mechanisms on mean Nusselt number are presented in Fig. 10 for $10 \leqslant Re \leqslant 40$ and $\phi = 5\%$. As expected, the mean Nusselt numbers decreased when Brownian and thermophoretic forces are ignored. It is worthy to mention that Brownian motion is more influential than the thermophoresis in enhancing the heat transfer rates. This indicates that the increase in particle-liquid interaction due to Brownian motion is a key mechanism for the enhancement in heat transfer seen in nanofluids. Finally, the mean Nusselt numbers obtained using DPM approach are compared with the results of SPM approach in Fig. 11. It is seen that the results of DPM vary significantly from that of the SPM approach and this variation is more pronounced at higher Reynolds numbers.

5.4. Distribution of particle concentration and particle trajectories

The spatial distributions of volume fraction of nanoparticles around the circular cylinder at $Re = 10$ and $40, d_p = 30$ nm and $\phi = 1\%, 3\%$ and 5% are presented in Fig. 12. It is to be mentioned that, the reflect boundary condition is used for the particles at cylinder surface and the Brownian force is ignored for better visualization. Completely contradicting to the assumption of SPM approach, it is seen that the distribution of nanoparticles is not uniform in the flow domain. The nanoparticle volume fraction distribution near the cylinder is non-homogeneous and the concentration in recirculation region is very less to zero. This indicates that the particles do not follow the streamlines in recirculation region. Only a very less volume fraction of particles enter the recirculation region. Due to increased momentum, majority of the nanoparticles tend to move in the main flow direction and do not enter the recirculation region. This results in very low concentration of nanoparticles in the recirculation region. The concentration in immediate proximity around the cylinder is also very less. But, strands of high volume fraction distribution is seen adjacent to the less concentration zone. The formation of this high concentration strands is perhaps due to the thermophoretic force that pushes the particle away from the hot cylinder and the reflect boundary condition for the particles at the cylinder surface. It is to be noted that, at $Re = 10$, this high concentration strands are stretched until the recirculation region. Whereas, at $Re = 40$, the strands are seen only in the proximity of cylinder. Also, at higher volume fractions, the particle concentration in the flow domain and the high concentration strands are high.This increased intensity of particle concentration is believed to result in better temperature distribution leading to higher heat transfer rates [54].

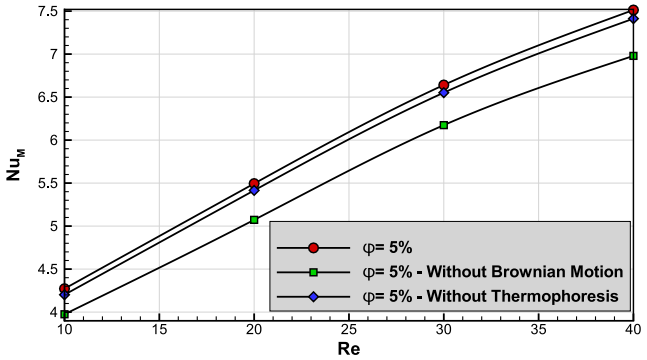

Fig. 10. Effect of Brownian motion and thermophoresis on mean Nusselt number (Nu_M) for Al_2O_3-H_2O ($\phi = 5\%$) nanofluid flow around a circular cylinder at $10 \leqslant Re \leqslant 40, d_p = 30$ nm and reflect boundary condition for the particles at cylinder surface.

The effect of Brownian motion on distribution of nanoparticles around the circular cylinder at $Re = 40, d_p = 30$ nm and $\phi = 5\%$ is shown in Fig. 13. It is seen that the inclusion of Brownian forces, resulted in more randomness of the nanoparticle distribution around the cylinder. The high concentration strands, which are noted when the Brownian motion was ignored, disappeared in the presence of Brownian motion. Thus, it is evident that the Brownian motion results in random motion of the nanoparticles and has a significant effect on the distribution of nanoparticles around the cylinder. This increase in randomness of the particle distribution in the flow domain due to Brownian motion can be related to the higher mean Nusselt numbers seen in Fig. 10, when the contribution of Brownian motion is accounted. Thus, it can be concluded that the Brownian motion results in random motion of the nanoparticles leading to intense particle-fluid interactions which thereby lead to enhanced heat transfer in nanofluids. Furthermore, it is noted that the inclusion of Brownian forces lead to diffusion of nanoparticles in the recirculation region. In the presence of Brownian force, an increase in concentration of nanoparticles is seen in the recirculation region close to the symmetry line. This increase in particle concentration near the rear stagnation point due to Brownian diffusion can be related to the sharp increase in local Nusselt number distribution with increase in particle volume fraction, observed close to the rear stagnation point (see Fig. 6).

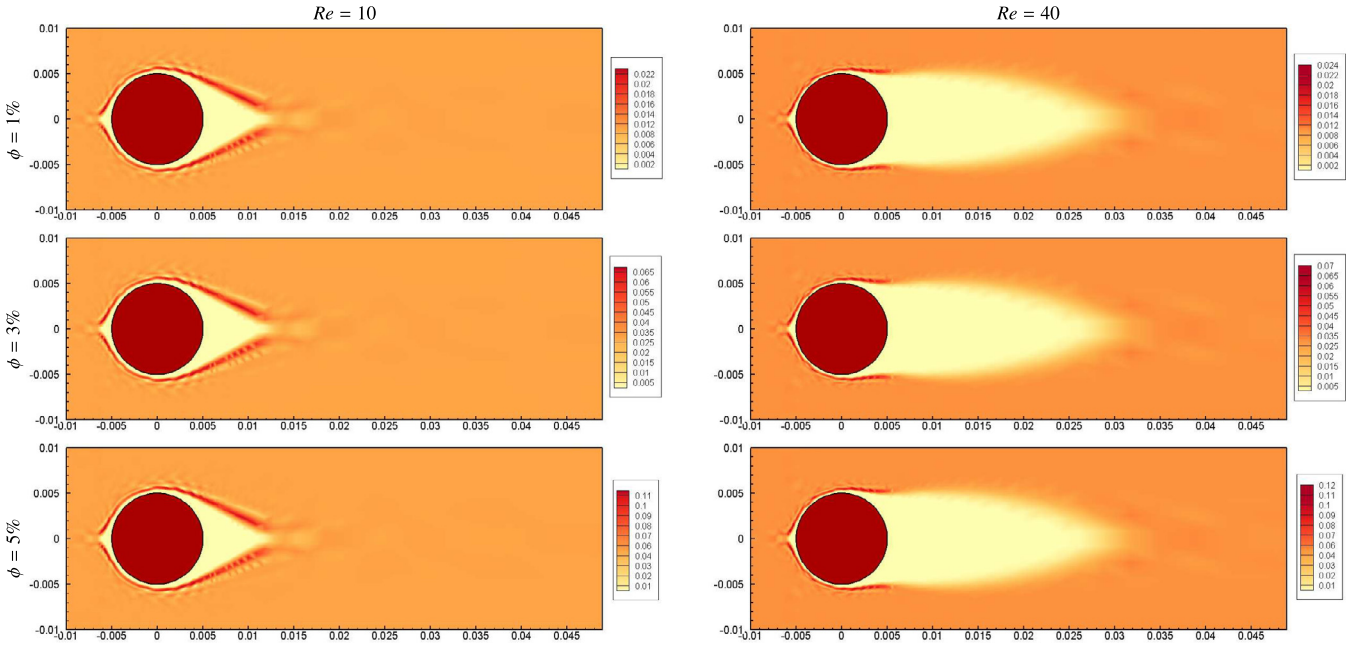

Fig. 12. Nanoparticle concentration distribution (without Brownian motion) around the circular cylinder for Al_2O_3-H_2O nanofluid flow at different volume fractions and $Re = 10$ and 40 with reflect boundary condition for the particles on cylinder surface and $d_p = 30$ nm.

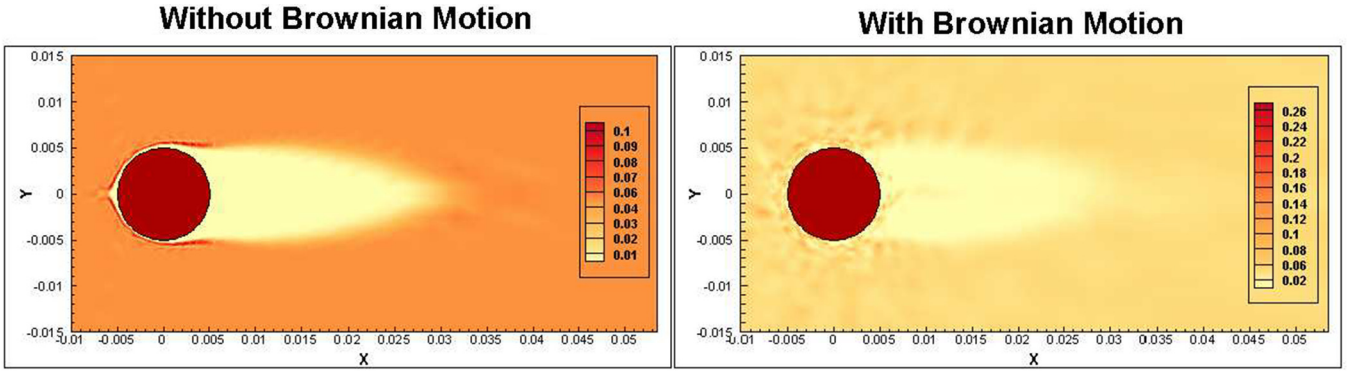

Fig. 13. Effect of Brownian motion on nanoparticle distribution around the circular cylinder for Al_2O_3-H_2O ($\phi = 5\%$) nanofluid flow at $Re = 40, d_p = 30$ nm and reflect boundary condition for the particles at cylinder surface.

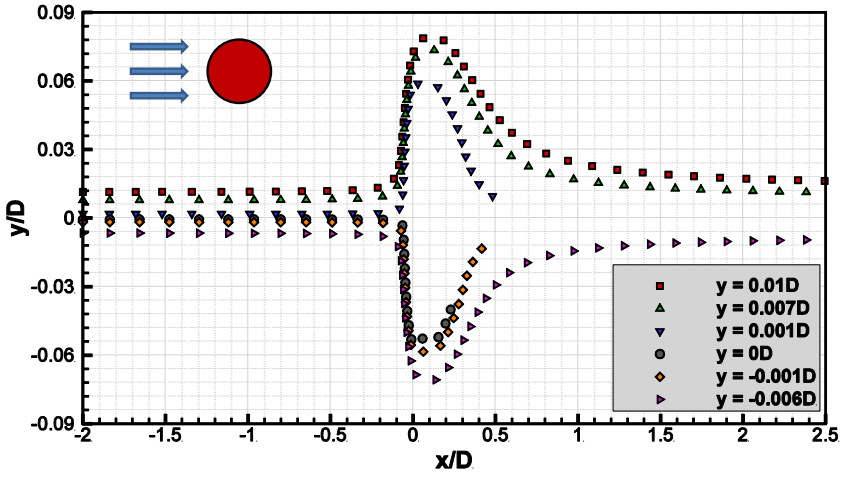

Fig. 14. Trajectories of nanoparticles (without Brownian motion) around the circular cylinder during Al_2O_3-H_2O ($\phi = 5\%$) nanofluid flow at $Re = 40, d_p = 30$ nm and reflect boundary condition for the particles at cylinder surface.

Fig. 14 shows the trajectories of nanoparticles at $\phi = 5\%, d_p = 30$ nm and $Re = 40$. Trajectories of 6 nanoparticles that were injected at different positions from the inlet are shown in this figure. It is to be noted that, the Brownian force is neglected here for better visualization of particle trajectories. In general, it is seen that the particles diverge above and below the cylinder which explains the formation of high concentration strands as seen Fig. 12. This may be due to the reflect boundary condition for the particles assumed at the cylinder surface and the thermophoretic force which pushes the particles away from the cylinder. The particles that start from $y = 0.01D, 0.007D$ and $-0.006D$ are comparatively away from the recirculation region and they continue to move in the direction of main flow. The other particles which respectively originate from $y = 0.001D, 0D$ and $-0.001D$ are closer to the recirculation region and are trapped in the recirculating wakes for a longer duration and hence, their trajectories are terminated in the recirculation region. This particle trajectories can be correlated with the different concentration zones seen in the flow domain.

6. Conclusions

Numerical simulations of forced convective heat transfer of Al_2O_3-H_2O nanofluid around a circular cylinder using a two-way coupled Eulerian-Lagrangian approach based Discrete Phase Modeling (DPM) were carried out. Influences of Reynolds number, particle volume fraction and diameter of nanoparticles on the heat transfer performance of nanofluids were investigated. Furthermore, special attention has been paid to the effects of Brownian motion and thermophoresis. In addition to that, the distribution of nanoparticles in the flow domain and the trajectories of particles are also discussed. The results of this numerical study can be summarized as follows:

- Obviously, nanofluids resulted in increased heat transfer rates than the basefluids.
- Higher heat transfer rates are obtained by increasing the flow Reynolds number.
- Nanofluids with smaller nanoparticles resulted in higher augmentation in heat transfer than the nanofluids with larger particles.
- Reflect and trap boundary conditions for the particles at the cylinder surface resulted in a marginal difference in heat transfer rates. Approximately, 1.5% higher heat transfer rate is seen while using reflect boundary condition.
- Local Nusselt number in the recirculation region is significantly influenced by the addition of nanoparticles.
- Brownian motion and thermophoresis play important roles in determining the heat transfer enhancement and particle distribution in nanofluids. The contribution of Brownian motion to the heat transfer augmentation is approximately 6% higher than that of the thermophoresis.
- Particle concentration sharply varies in the region close to the cylinder and in the recirculation region.
- Brownian motion results in random distribution of nanoparticles in the region close to the cylinder.
- The results of DPM study vary notably from the results of SPM approach and it is believed that the results of DPM are more accurate due to its realistic assumptions. It is to be noted that, it is arbitrarily assumed that the particle distribution is uniform through out the domain in SPM approach.

The effects of nanoparticle concentration on heat transfer performance of nanofluids is expected to be more pronounced in unsteady and buoyancy driven flow scenarios. In future, a detailed study on particle concentration and heat transfer using nanofluids in mixed and natural convective flows using two-way coupled Eulerian-Lagrangian approach can be carried out.

Acknowledgments

One of the authors, S. Dhinakaran, gratefully acknowledges the financial aid received from Science and Engineering Research Board, Department of Science and Technology (DST), Government of India through a project grant (Project Reference No. SB/FTP/ETA-427/2012) for carrying out this work. The authors are highly obliged to the reviewers for their insightful comments and suggestions.

Conflict of interest

None.

References

[1] R.P. Bharti, R.P. Chhabra, V. Eswaran, Steady forced convection heat transfer from a heated circular cylinder to power-law fluids, Int. J. Heat Mass Transf. 50 (5) (2007) 977–990.
[2] C.F. Lange, F. Durst, M. Breuer, Momentum and heat transfer from cylinders in laminar crossflow at $10^{-4} \leq Re \leq 200$, Int. J. Heat Mass Transf. 41 (22) (1998) 3409–3430.
[3] V.T. Morgan, The overall convective heat transfer from smooth circular cylinders, Adv. Heat Transf. 11 (1975) 199–264.
[4] C.H.K. Williamson, Vortex dynamics in the cylinder wake, Annu. Rev. Fluid Mech. 28 (1) (1996) 477–539.
[5] M.M. Zdravkovich, Flow Around Circular Cylinders, Applications, vol. 5, Oxford University Press, 2003, ISBN 0 19 (856561).
[6] G. Saha, M.C. Paul, Numerical analysis of the heat transfer behaviour of water based Al_2O_3 and TiO_2 nanofluids in a circular pipe under the turbulent flow condition, Int. Commun. Heat Mass Transf. 56 (2014) 96–108.
[7] M.S. Valipour, A.Z. Ghadi, Numerical investigation of fluid flow and heat transfer around a solid circular cylinder utilizing nanofluid, Int. Commun. Heat Mass Transf. 38 (9) (2011) 1296–1304.
[8] R.L. Hamilton, O.K. Crosser, Thermal conductivity of heterogeneous two-component systems, Ind. Eng. Chem. Fundam. 1 (3) (1962) 187–191.
[9] H.C. Brinkman, The viscosity of concentrated suspensions and solutions, J. Chem. Phys. 20 (4) (1952) 571.
[10] M.S. Valipour, R. Masoodi, S. Rashidi, M. Bovand, M. Mirhosseini, A numerical study on convection around a square cylinder using $Al_2O_3 - H_2O$ nanofluid, Therm. Sci. 18 (4) (2014) 1305–1314.
[11] M. Vegad, S. Satadia, P. Pradip, P. Chirag, P. Bhargav, Heat transfer characteristics of low Reynolds number flow of nanofluid around a heated circular cylinder, Proc. Technol. 14 (2014) 348–356.
[12] J.C.M. Garnett, Colours in metal glasses, in metallic films, and in metallic solutions. II, Philos. Trans. Roy. Soc. Lond. Ser. A Containing Pap. Math. Phys. Charact. (1906) 237–288.
[13] E. Abu-Nada, K. Ziyad, M. Saleh, Y. Ali, Heat transfer enhancement in combined convection around a horizontal cylinder using nanofluids, J. Heat Transf. 130 (8) (2008) 084505.
[14] R.T.H. Bing, H.A. Mohammed, Upward laminar flow around a circular cylinder using nanofluids, J. Purity Utility React. Environ. 1 (2012) 435–450.
[15] V. Etminan-Farooji, E. Ebrahimnia-Bajestan, H. Niazmand, S. Wongwises, Unconfined laminar nanofluid flow and heat transfer around a square cylinder, Int. J. Heat Mass Transf. 55 (5) (2012) 1475–1485.
[16] A.J. Chamkha, A. Rashad, A.M. Aly, Transient natural convection flow of a nanofluid over a vertical cylinder, Meccanica 48 (1) (2013) 71–81.
[17] S. Sarkar, A. Dalal, G. Biswas, Unsteady wake dynamics and heat transfer in forced and mixed convection past a circular cylinder in cross flow for high Prandtl numbers, Int. J. Heat Mass Transf. 54 (15) (2011) 3536–3551.
[18] S. Sarkar, S. Ganguly, G. Biswas, Mixed convective heat transfer of nanofluids past a circular cylinder in cross flow in unsteady regime, Int. J. Heat Mass Transf. 55 (17) (2012) 4783–4799.
[19] S. Sarkar, S. Ganguly, A. Dalal, Buoyancy driven flow and heat transfer of nanofluids past a square cylinder in vertically upward flow, Int. J. Heat Mass Transf. 59 (2013) 433–450.
[20] S. Sarkar, S. Ganguly, A. Dalal, P. Saha, S. Chakraborty, Mixed convective flow stability of nanofluids past a square cylinder by dynamic mode decomposition, Int. J. Heat Fluid Flow 44 (2013) 624–634.
[21] S. Sarkar, S. Ganguly, A. Dalal, Analysis of entropy generation during mixed convective heat transfer of nanofluids past a rotating circular cylinder, J. Heat Transf. 136 (6) (2014) 062501.
[22] Y. Xuan, Q. Li, Heat transfer enhancement of nanofluids, Int. J. Heat Fluid Flow 21 (1) (2000) 58–64.

[23] A. Behzadmehr, M. Saffar-Avval, N. Galanis, Prediction of turbulent forced convection of a nanofluid in a tube with uniform heat flux using a two phase approach, Int. J. Heat Fluid Flow 28 (2) (2007) 211–219.
[24] A. Akbarinia, R. Laur, Investigating the diameter of solid particles effects on a laminar nanofluid flow in a curved tube using a two phase approach, Int. J. Heat Fluid Flow 30 (4) (2009) 706–714.
[25] M. Alinia, D.D. Ganji, M. Gorji-Bandpy, Numerical study of mixed convection in an inclined two sided lid driven cavity filled with nanofluid using two-phase mixture model, Int. Commun. Heat Mass Transf. 38 (10) (2011) 1428–1435.
[26] M. Esfandiary, B. Mehmandoust, A. Karimipour, H.A. Pakravan, Natural convection of Al_2O_3-water nanofluid in an inclined enclosure with the effects of slip velocity mechanisms: Brownian motion and thermophoresis phenomenon, Int. J. Therm. Sci. 105 (2016) 137–158.
[27] O. Ghaffari, A. Behzadmehr, H. Ajam, Turbulent mixed convection of a nanofluid in a horizontal curved tube using a two-phase approach, Int. Commun. Heat Mass Transf. 37 (10) (2010) 1551–1558.
[28] M. Goodarzi, M.R. Safaei, K. Vafai, G. Ahmadi, M. Dahari, S.N. Kazi, N. Jomhari, Investigation of nanofluid mixed convection in a shallow cavity using a two-phase mixture model, Int. J. Therm. Sci. 75 (2014) 204–220.
[29] R. Lotfi, Y. Saboohi, A.M. Rashidi, Numerical study of forced convective heat transfer of nanofluids: comparison of different approaches, Int. Commun. Heat Mass Transf. 37 (1) (2010) 74–78.
[30] S. Mirmasoumi, A. Behzadmehr, Numerical study of laminar mixed convection of a nanofluid in a horizontal tube using two-phase mixture model, Appl. Therm. Eng. 28 (7) (2008) 717–727.
[31] R.M. Moghari, A. Akbarinia, M. Shariat, F. Talebi, R. Laur, Two phase mixed convection Al_2O_3-water nanofluid flow in an annulus, Int. J. Multiph. Flow 37 (6) (2011) 585–595.
[32] H.A. Pakravan, M. Yaghoubi, Analysis of nanoparticles migration on natural convective heat transfer of nanofluids, Int. J. Therm. Sci. 68 (2013) 79–93.
[33] G. Saha, M.C. Paul, Heat transfer and entropy generation of turbulent forced convection flow of nanofluids in a heated pipe, Int. Commun. Heat Mass Transf. 61 (2015) 26–36.
[34] M. Siavashi, M. Jamali, Heat transfer and entropy generation analysis of turbulent flow of TiO_2-water nanofluid inside annuli with different radius ratios using two-phase mixture model, Appl. Therm. Eng. 100 (2016) 1149–1160.
[35] R. Deepak Selvakumar, S. Dhinakaran, Forced convective heat transfer of nanofluids around a circular bluff body with the effects of slip velocity using a multi-phase mixture model, Int. J. Heat Mass Transf. 106 (2017) 816–828.
[36] V. Bianco, F. Chiacchio, O. Manca, S. Nardini, Numerical investigation of nanofluids forced convection in circular tubes, Appl. Therm. Eng. 29 (17) (2009) 3632–3642.
[37] H. Afshar, M. Shams, S.M.M. Nainian, G. Ahmadi, Microchannel heat transfer and dispersion of nanoparticles in slip flow regime with constant heat flux, Int. Commun. Heat Mass Transf. 36 (10) (2009) 1060–1066.
[38] H. Aminfar, R. Motallebzadeh, Investigation of the velocity field and nanoparticle concentration distribution of nanofluid using Lagrangian-Eulerian approach, J. Disper. Sci. Technol. 33 (1) (2012) 155–163.
[39] H. Bahremand, A. Abbassi, M. Saffar-Avval, Experimental and numerical investigation of turbulent nanofluid flow in helically coiled tubes under constant wall heat flux using Eulerian-Lagrangian approach, Powder Technol. 269 (2015) 93–100.
[40] S. Rashidi, M. Bovand, J.A. Esfahani, G. Ahmadi, Discrete particle model for convective Al_2O_3-water nanofluid around a triangular obstacle, Appl. Therm. Eng. 100 (2016) 39–54.
[41] Y. He, Y. Men, Y. Zhao, H. Lu, Y. Ding, Numerical investigation into the convective heat transfer of TiO_2 nanofluids flowing through a straight tube under the laminar flow conditions, Appl. Therm. Eng. 29 (10) (2009) 1965–1972.
[42] S. Tahir, M. Mital, Numerical investigation of laminar nanofluid developing flow and heat transfer in a circular channel, Appl. Therm. Eng. 39 (2012) 8–14.
[43] M. Bovand, S. Rashidi, G. Ahmadi, J.A. Esfahani, Effects of trap and reflect particle boundary conditions on particle transport and convective heat transfer for duct flow-a two-way coupling of Eulerian-Lagrangian model, Appl. Therm. Eng. 108 (2016) 368–377.
[44] C.T. Crowe, Multiphase Flow Handbook, vol. 59, CRC Press, 2005.
[45] W.J. Minkowycz, E.M. Sparrow, J.Y. Murthy, J.P. Abraham, Handbook of Numerical Heat Transfer, John Wiley & Sons, Inc., 2009.
[46] A. Li, G. Ahmadi, Dispersion and deposition of spherical particles from point sources in a turbulent channel flow, Aerosol Sci. Technol. 16 (4) (1992) 209–226.
[47] M. Mahdavi, M. Sharifpur, J.P. Meyer, CFD modelling of heat transfer and pressure drops for nanofluids through vertical tubes in laminar flow by Lagrangian and Eulerian approaches, Int. J. Heat Mass Transf. 88 (2015) 803–813.
[48] W. Ranz, W. Marshall, Evaporation from drops, Chem. Eng. Prog. 48 (3) (1952) 141446.
[49] C. Wu, A. Berrouk, Discrete particle model for dense gas-solid flows, Adv. Multiph. Flow Heat Transf. 3 (2012) 151.
[50] S.C.R. Dennis, G.-Z. Chang, Numerical solutions for steady flow past a circular cylinder at Reynolds numbers up to 100, J. Fluid Mech. 42 (3) (1970) 471–489.
[51] A.A. Soares, J.M. Ferreira, R.P. Chhabra, Flow and forced convection heat transfer in crossflow of non-Newtonian fluids over a circular cylinder, Ind. Eng. Chem. Res. 44 (15) (2005) 5815–5827.
[52] R.D. Selvakumar, S. Dhinakaran, Nanofluid flow and heat transfer around a circular cylinder: a study on effects of uncertainties in effective properties, J. Mol. Liq. 223 (2016) 572–588.
[53] T.P. Teng, Y.H. Hung, T.C. Teng, H.E. Mo, H.G. Hsu, The effect of alumina/water nanofluid particle size on thermal conductivity, Appl. Therm. Eng. 30 (14) (2010) 2213–2218.
[54] M. Karimzadehkhouei, S.E. Yalcin, K. Şendur, M.P. Mengüç, A. Koşar, Pressure drop and heat transfer characteristics of nanofluids in horizontal microtubes under thermally developing flow conditions, Exp. Therm. Fluid Sci. 67 (2015) 37–47.